Hindawi
Journal of Nanomaterials
Volume 2023, Article ID 1722978, 11 pages
https://doi.org/10.1155/2023/1722978

Research Article

Improving the Photo Electro Catalytic Degradation of Methylene Blue by Modified TiO_2/ITO Photo Anodes

Jihad Alsaleh Almohammad,[1] **Mohammad Hashem**,[1] **Hanan Alchaghouri**,[1] **and Ibrahim Alghoraibi**[2,3]

[1]*Department of Chemistry, Faculty of Sciences, Damascus University, Damascus, Syria*
[2]*Department of Physics, Faculty of Sciences, Damascus University, Damascus, Syria*
[3]*Faculty of Pharmacy, Arab International University, Damascus, Syria*

Correspondence should be addressed to Jihad Alsaleh Almohammad; jihad.mohammad@damascusuniversty.edu.sy and Ibrahim Alghoraibi; ibrahim.alghoraibi@gmail.com

Received 3 February 2023; Revised 3 May 2023; Accepted 29 May 2023; Published 15 June 2023

Academic Editor: Osman Ahmed Zelekew

TiO_2 photoanodes have gained significant attention for the removal of organic pollutants through photoelectrocatalytic processes, with the aim of developing a cost-effective and efficient method for improving the degradation of pollutants in surface water. This study investigated the effects of adding titanium nanooxide (Degussa P25) containing 70% anatase and 30% rutile phases on the properties of nanostructured TiO_2 photoanodes prepared on glass substrates (indium tin oxide (ITO)) using sol–gel/dip coating techniques The results obtained from ultraviolet–visible transmittance spectroscopy, electrochemical (EC) impedance spectroscopy, photocurrent, and atomic force microscopy analyses revealed that the addition of Degussa P25 improved the electrical conductivity of the TiO_2/ITO anode and reduced the optical bandgap from 3.50 to 3.35 eV, while the size of the titanium oxide particles decreased to about 75 nm. The EC impedance spectra measurement confirms that the addition of titanium nanooxide Degussa P25 improved the electrical conductivity for TiO_2/ITO anode. The photoelectrocatalysis (PEC) performance of the TiO_2 photoanodes was investigated via the degradation of methylene blue (MB) under UVA light irradiation. The AB photoanode (with the addition of Degussa P25) exhibited excellent PEC performance, with 95.9% color removal efficiency and 63% total organic carbon (TOC) removal efficiency, compared to 92% color removal efficiency and 56% TOC removal efficiency for the A photoanode (without the addition of Degussa P25). The kinetic constants (k) were 134×10^{-4}, 110×10^{-4} (min^{-1}) for A and AB anodes, respectively, and the degradation of MB followed first-order kinetics for all anodes. The A and AB anodes were compared as electrodes for the degradation of MB using PEC, photocatalysis (PC), and EC technologies. Subsequently, The A and AB anodes were utilized as electrodes to compare the performance of PEC, PC, and EC technologies for the degradation of MB. The results showed that the AB anode exhibited higher efficiency in all PC technologies, with color removal (%) efficiencies of 95.9% (PEC), 33% (PC), and 21% (EC) compared to 92% (PEC), 28% (PC), and 19% (EC) for the A anode. Additionally, the photooxidation process had a 2.1% effect on the degradation of the initial MB concentration.

1. Introduction

Searching for solutions to the environmental pollution problem that is exacerbating day after day is an urgent need on the global stage. Huge amounts of pollutants generated from pharmaceutical and industrial processes have been discovered to have harmful and long-term impacts on our daily life [1–4]. Some of them are difficult to degrade due to their complex compositions, resulting in harmful residual pollutants in water [3, 5]. Several technologies and strategies, that are efficient and environmentally friendly, have been applied to the degradation of these pollutants, such as Fenton's reaction [6], biological methods [7], and chemical oxidation [8]. However, these methods are often not energy efficient, or they secondarily pollute during the degradation of the primary waste since they are based on conventional wastewater treatments [3]. In this regard, photoelectrocatalysis (PEC), which is one of the most recent electrochemical (EC) advanced oxidation processes technology, offers a promising, efficient, and environmentally friendly approach for

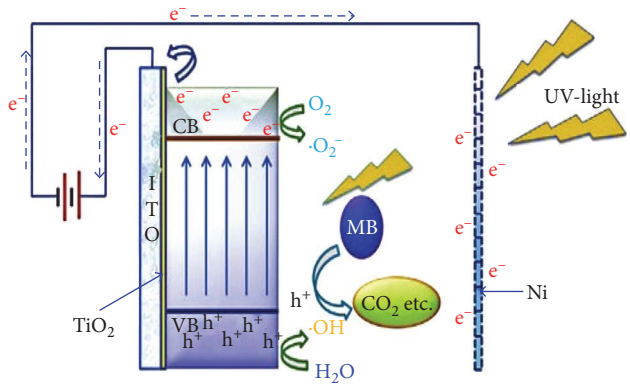

FIGURE 1: Mechanism of photoelectrocatalytic degradation of MB using TiO_2/ITO anode and the reactions that occur at the surface.

removing a wide spectrum of organic pollutants from wastewater and reduce the incidence of charge recombination and partially improve the limitations of photocatalysis (PC), which it uses suitable semiconducting materials as photoanodes [2–4, 9, 10]. Another interesting advantage of PEC is lower energy consumption when compared to anodic oxidation, which requires high potential/current to facilitate the degradation of organic [2]. In PEC, it is applying an external potential to a photocatalyst film supported on a conductive substrate that electrochemically aids the photocatalytic process. Through PC, the substrate helps expel the electrons that reach the conduction band (e^-_{CB}) toward the external circuit, resulting a significant reduction in the challenge of rapid and spontaneous recombination of charge carriers (e^-_{CB}/h^+_{VB}) that is peculiar to PC and producing an increase in the electron transfer rate [3, 9, 10], as shown in Figure 1. Further, the holes generated in the valence band (h^+_{VB}) react with water to produce ($^{\cdot}OH$), the second strongest oxidant known after fluorine, which nonselectively reacts with most organics in water [4, 5, 9, 10]. When this technique is used to treat water contaminated with recalcitrant organic molecules, such as pharmaceuticals, total mineralization to water and carbon dioxide can be achieved over a period of time, or the molecules can be broken down to nontoxic organic molecules within a short period of time [3]. In other words, the efficiency of PEC in the degradation of organic pollutants in aqueous medium depends on the ability of photoanodes into generate in situ oxidizing reactive oxygen species [9–13]. Thus, the materials used to prepare a photoanode are an important factor in the photoelectrocatalytic process [11–14]. Figure 1 shows the mechanism of the photoelectron catalytic process using the TiO_2/indium tin oxide (ITO) anode and the reactions that occur on the surface.

The preparation of stable and reusable photocatalysts on conductive materials as a support is one of the most important steps in the development of PEC technology. Several kinds of semiconductors, particularly TiO_2, remained the most applied semiconducting photocatalyst as anodic material for photoelectrocatalytic degradation of organic compounds in water [2, 3]. TiO_2 is widely recognized as a favorable catalyst in the preparation of photoelectrodes for its advantages of nontoxicity, high reactivity, cost-effectiveness, easy synthesis, and chemical inertness [9, 10, 13]. TiO_2 occurs in three polymorphs, the stable rutile, metastable anatase, and brookite, showing different properties and bandgaps, i.e., 3.0, 3.22, and 3.23 eV, respectively [14]. Anatase reveals higher photocatalytic activity than rutile and brookite in many cases due to different lattice structures and electronic band structures [15].

Titanium oxide nanoparticles films can be prepared by several methods, such as magnetron sputtering [16], chemical vapor deposition [17], electrophoretic deposition (EPD) [10] sol–gel, dip-coating, spin-coating [9, 10], atomic layer deposition [18], and atmospheric plasma spray [19]. However, the sol–gel method is the most popular technique to synthesize TiO_2 thin-film photocatalysts [20] because it is an easy, simple, and cost-effective method that can be applied to all types of piles and sizes. In addition, it is a method that allows obtaining photoelectrodes with large internal surfaces, EC stability, and a high efficiency for the removal of organic pollutants and allows to achieve enough crystallinity to provide TiO_2 the desired combination of mechanical, catalytic, and optoelectronic properties, allowing it to achieve degradation efficiencies of contaminants between 70% and 100% during short treatment times [9]. All these techniques have been studied using different conductive substrates such as ITO, fluorine-doped tin oxide, titanium, stainless steel (SS), and recently boron-doped diamond (BDD) [2, 3, 9, 10, 21–24]. ITO-coated glass is made by spreading a thin and uniform layer of ITO over a glass substrate, making the glass have advantages (low resistance and highly transparent). Thus, the photoanode on an ITO glass (as a current conducting substrate) has a high efficiency for optical photons to pass through to generate holes and reduces the complexity of the processing unit. Many methods have been studied to improve the photocatalytic properties, such as doping with transition metals oxide [25] and noble metals [26, 27]. Doping with P25 is an effective and simple strategy for preparing and improving photocatalysts and enhancing the ability to degrade pollutants [28–30]. Sigcha-Pallo et al. [10] have used the EPD for papering a photoanode of titanium dioxide (TiO_2) nanoparticles (Degussa P25) onto a BDD substrate, applied in the degradation and mineralization of sodium diclofenac (DCF-Na) in an aqueous medium using PEC. The degradation and mineralization efficiencies of pollutants were between 80% and 100% during short treatment times [10]. The TiO_2/P25/ITO photoanode is one of the most promising photoanodes in PEC for wastewater treatment. The combination of the fabrication methods with sol–gel is an effective strategy to overcome the weaknesses of applying the sol–gel alone. Many studies have been concerned on the combination of the sol–gel with other techniques, for example, Carreño-Lizcano et al. [31] have prepared nitrogen-doped TiO_2/rGO (reduced graphene oxide) films by a sol–gel method and immobilized on SS by dip-coating technique to evaluate their photoelectrocatalytic activity in the phenol oxidation. The efficient phenol degradation was around 45% by using photoelectrocatalysis in comparison with other oxidation process as photolysis (1.5%), PC (21%), and electrocatalysis (24%) [31]. Alulema-Pullupaxi et al. [9] have combined sol–gel/spin-coating methods to synthesize a robust and stable (TiO_2/BDD) photoanode for studying the degradation of

glyphosate by EC oxidation on BDD and photoelectrocatalysis on TiO_2/BDD in dark and ultraviolet (UV) light conditions. The glyphosate degradation was 2.3 times faster by photoelectrocatalysis on TiO_2/BDD relative to BDD.

Therefore, this work proposes the synthesis of TiO_2/ITO using a novel method combining sol–gel/dip-coating techniques with the addition of titanium nanooxide (Degussa P25).

The aim of this study is investigating the effect of adding Degussa P25 during the preparation of the photoanode on the surface morphology, EC, optical properties, and applying PEC technology to the degradation of methylene blue (MB). In addition, this study highlights the addition of P25 powders to a TiO_2/P25/ITO photoanode to improve the PEC performance, efficiency degradation of MB, operational ability, and enhance photocatalyst activity of the photoanode.

2. Experimental

2.1. Materials. According to the manufacturer's specifications, Titanium dioxide (Degussa P25) comprises 70% anatase and 30% rutile phases, with an average particle size of this compound is approximately 25 nm and it exhibits a specific surface area of 48.3 $m^2 g^{-1}$ from N_2 adsorption at 77 K.

The following source: (MB, C.I.52015) from Scharlau Company (Barcelona-Spain) was used to prepare the artificially contaminated solutions of MB without any additional purification processes. Sodium sulfate Na_2SO_4 (95.0%) was purchased from Riedel_de Haen company, and used in the preparation of sol–gel titanium tetra isopropoxide (TTIP) purity, (97.0%), $M = 284.22$ and Triton X-100 from Scharlau Chemie, laboratory grade, $M = 646.37\,g\,mol^{-1}$, $D = 1.07\,g\,cm^{-3}$, (Germany), ethanol from BDH (Germany) purity (99.2%), $M = 46.01$, and acetic acid from PRS (Spain) purity (98%). ITO glass of 50 Ω resistance, dimensions (3–10 cm), and thickness of 0.07 cm was bought from Aldrich (Germany). In addition, a cathode of nickel metal from Aldrich (Germany). Water for injections was also used in preparing samples and solutions.

2.2. Characterization. The morphology of the TiO_2 nanoparticles was characterized by an atomic force microscopy (AFM) (esayScan2, nanosurf), UV–visible (UV–Vis) spectroscopy studies were performed in order to determine the optical properties for wavelengths ranging from 300 to 800 nm using a Varian Carry 5000 (UV–VIS-IR), A UV–Vis spectrophotometer and total organic carbon (TOC) (Phoenix8000) were employed to monitor the degradation of MB. The point of zero charge pH_{pzc}, was determined by acid–base titration method following the procedure adopted previously [32] for a powder sample. The electrochemical impedance spectroscopy (EIS) was measured using an IVIUM-STAT.XR Potentiostat/Galvanostat with integrated high-performance frequency response analyzers for EIS measurements. With an excitation signal of 10 mV amplitude. The impedance vs frequency spectra was acquired at the open circular potential of the system in the dark and under UV illumination. The photocurrent densities were examined by linear sweep voltammetry measurements in a three-electrode EC system, using an Ag/AgCl as the reference electrode and Pt mesh as the counter electrode in a 1 M NaOH electrolyte.

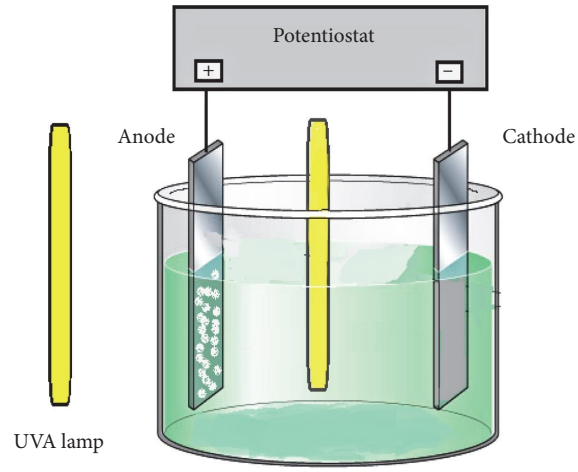

Figure 2: Scheme of the unit used in the treatment.

2.3. Preparation of Photoanodes. Solution A was prepared by adding 1.5 mL surfactant agent Triton X-100, 10.2 mL acetic acid, 57 mL ethanol, and 5.4 mL TTIP and kept under vigorous stirring by ultrasonication for 3 hr. Solution B was prepared by adding 1 g titanium oxide (Degussa P25) to 10 mL of ethanol and 10 mL of water solution under continuous ultrasonic stirring. Solution B was added dropwise to solution A with constant stirring for a period of 1 hr to obtain solution AB.

ITO glass slides were rinsed with water and ethanol, calcined at 550°C to remove any impurities from the surface, and then immersed so that 8 cm from the conductor side was wetted by the sol via using the dipping electroplating device in solution A to obtain the photoanode A and another one in solution AB to obtain the photoanode AB. By programing the immersion time of 1 s and the drawing speed of 100 $\mu m\,s^{-1}$. Finally, the heat treatment takes place in two stages. The first stage raised the temperature to 100°C for 3 hr, and then the temperature was raised to 450°C at a speed of 15°C s^{-1}. The temperature was kept for 2 hr and then cooled down while maintaining the previous speed.

2.4. PEC Degradation of MB. The PEC degradation of MB was carried out in a homemade single-compartment cuboid transparent glass reactor Figure 2. In the PEC experiments, A and AB photoanodes acted as photoelectrodes and the Ni foils as cathodes (the geometric area in contact with the MB solution was 48 cm^2). The distance between the two electrodes was 3.0 cm. The UVA light was supplied by two lamps; the first lamp ($\lambda = 365$ nm, 12 T5, 6 W, OSRAM, made in Italy) was placed inside the reactor parallel to the two electrodes. The second lamp ($\lambda = 365$ nm, 12 T8, 8 W, Hitachi, made in Japan) was placed outside the reactor and parallel to the two electrodes. A cooling water recirculation system was equipped to control the experimental temperature at 25°C. The distance between the inside lamp and the photoelectrode was 2 cm, and distance between the outside lamp and the photoelectrode was 6 cm. The concentration of MB was set as 25 mg L^{-1}, and 0.05 M of Na_2SO_4 was added to enhance the MB solution conductivity. Prior to irradiation, the two electrodes were

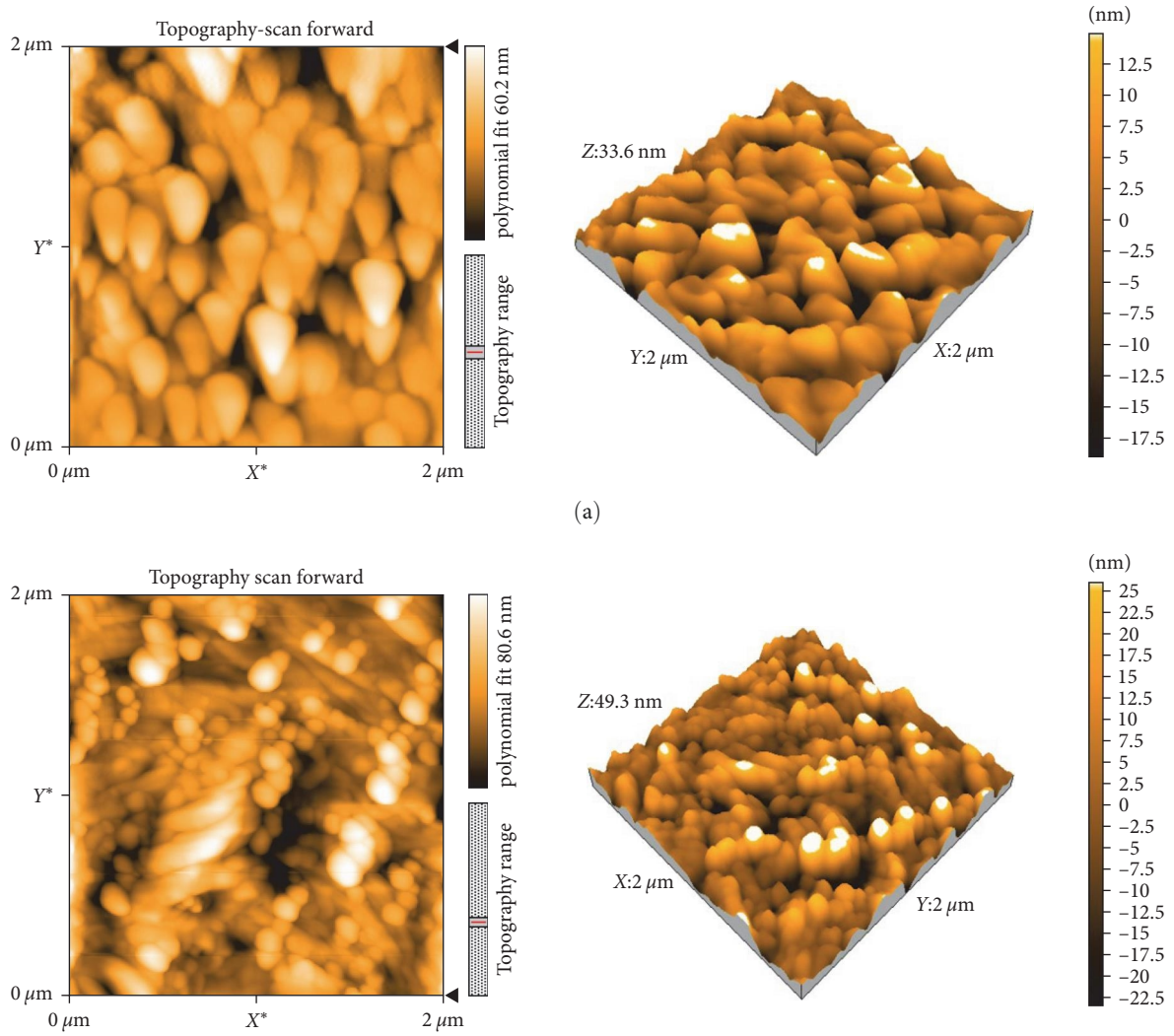

FIGURE 3: AFM 2D and 3D images ($2 \times 2\,\mu m^2$) for photoanode A (a) and photoanode AB (b).

vertically fixed in the reactor. Then 200 mL of MB is added to the reactor and stirred in the dark for 30 min to establish adsorption–desorption equilibrium. The potential in the PEC was controlled by a DC power supply. Samples were taken at specified intervals to follow the change of concentrations of solutions during treatment.

The removal efficiency is calculated as follows:

$$\text{Removal}\,(\%) = \frac{C_0 - C}{C_0} \times 100, \tag{1}$$

where C_0, C (mg L^{-1}) the MB concentration initial and during the treatment process.

3. Results and Discussion

3.1. Characterization of TiO_2/ITO Anode. The AFM micrographs of TiO_2/ITO thin films deposited at room temperature after immersing in solutions A and AB are shown in Figure 3.

From AFM images, it is observed nonuniform unequal distribution grains were formed with a huge grain diameter of 125 nm, average area surface roughness (Sa = 20.2 nm), and area root-mean-square roughness (Sqrms = 31.1 nm) after immersing in solution A, while the grain carpet after immersing in solution AB showed homogeneous spherical shape formed on the surface of the film. The grains had relatively low narrow size distributions with low mean diameter ($D = 75$ nm) and high (Sa = 28.6 nm) and (Sqrms = 35.0 nm), respectively. In the case of formation, the thin film after the deposition of TiO_2 from solution AB. The film deposited from solution AB gave a better performance as a photoanode, and this is due to the fact that TiO_2 thin film on ITO has a good quality, high surface roughness, uniform, and completely covered the entire substrate surface area.

Comparing the grains size distribution histogram of A and AB thin films (as seen in Figure 4), we found that the film formed with solution (AB) is the most suitable case to form nanograins of TiO_2 with a small diameter and narrow size distribution which ranged from 30 to 185 nm. On the

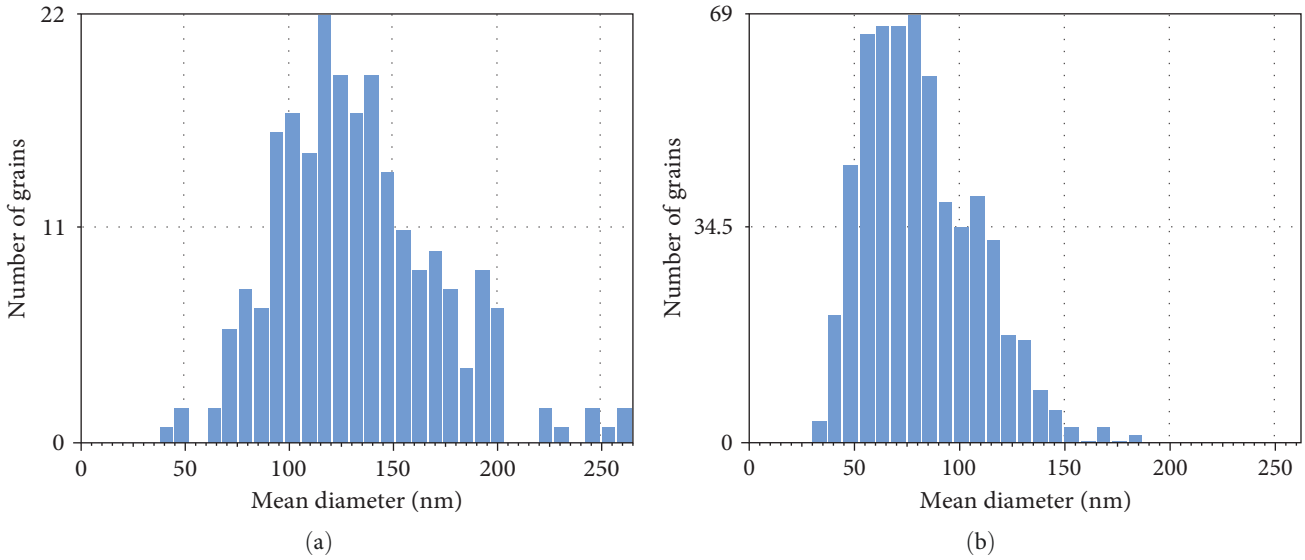

Figure 4: Grains size distribution histogram of photoanodes A (a) and AB (b).

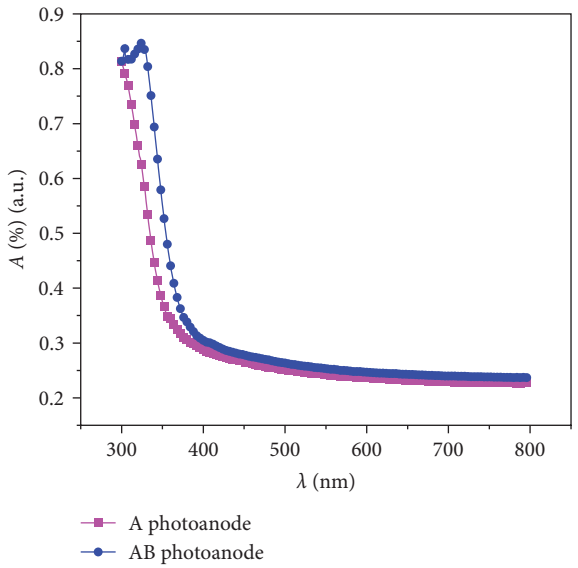

Figure 5: Optical absorbance spectra of A (a) and AB (b) photoanodes.

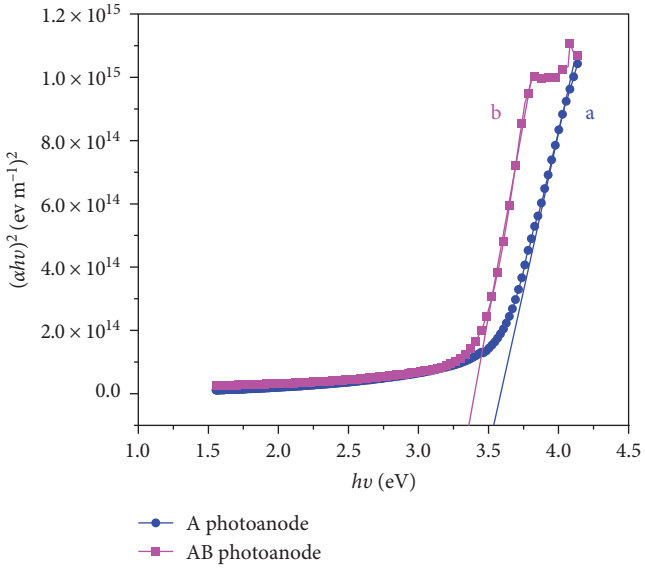

Figure 6: Calculation of E_g in A (a) and AB (b) photoanodes.

other hand, the TiO_2/ITO thin films prepared with solution A exhibit a large distribution and varied from 42 to 265 nm. The difference in grain size could be attributed to the presence of addition (Degussa P25) with nanoscale dimensions in solution AB, which affected the grain size formed during calcination.

3.2. Optical Properties. Absorbance measurements of anodes, Figure 5, were recorded in the range of 300–800 nm using a UV–Vis spectrophotometer (Varian carry 5000), allowing the calculation of the thickness and bandgap of A and AB photoanodes. The absorption coefficient was calculated using the relation $\alpha = \ln(1/T)/t$ [33], where T is the transmittance and t is the thickness of the TiO_2 film. The thickness of the film was also calculated optically using a He–Ne laser. Tauc's model is used for the optical bandgap's (E_g) calculations [34]:

$$(\alpha h\nu) = A\left(h\nu - E_g\right)^n, \tag{2}$$

where α, h, A, and ν represent the absorption coefficient, Planck's constant, constant of proportionality, and frequency of light, respectively. $n = 1/2$ and two for indirect and direct transition, respectively [35]. Bandgap energy for A and AB anodes are determined by a slope of the curves on the x-axis, as exhibited as shown in Figure 6.

The bandgap energy was reduced from $E_g = 3.52$ to 3.35 eV when we added Degussa P25, which is closer to the

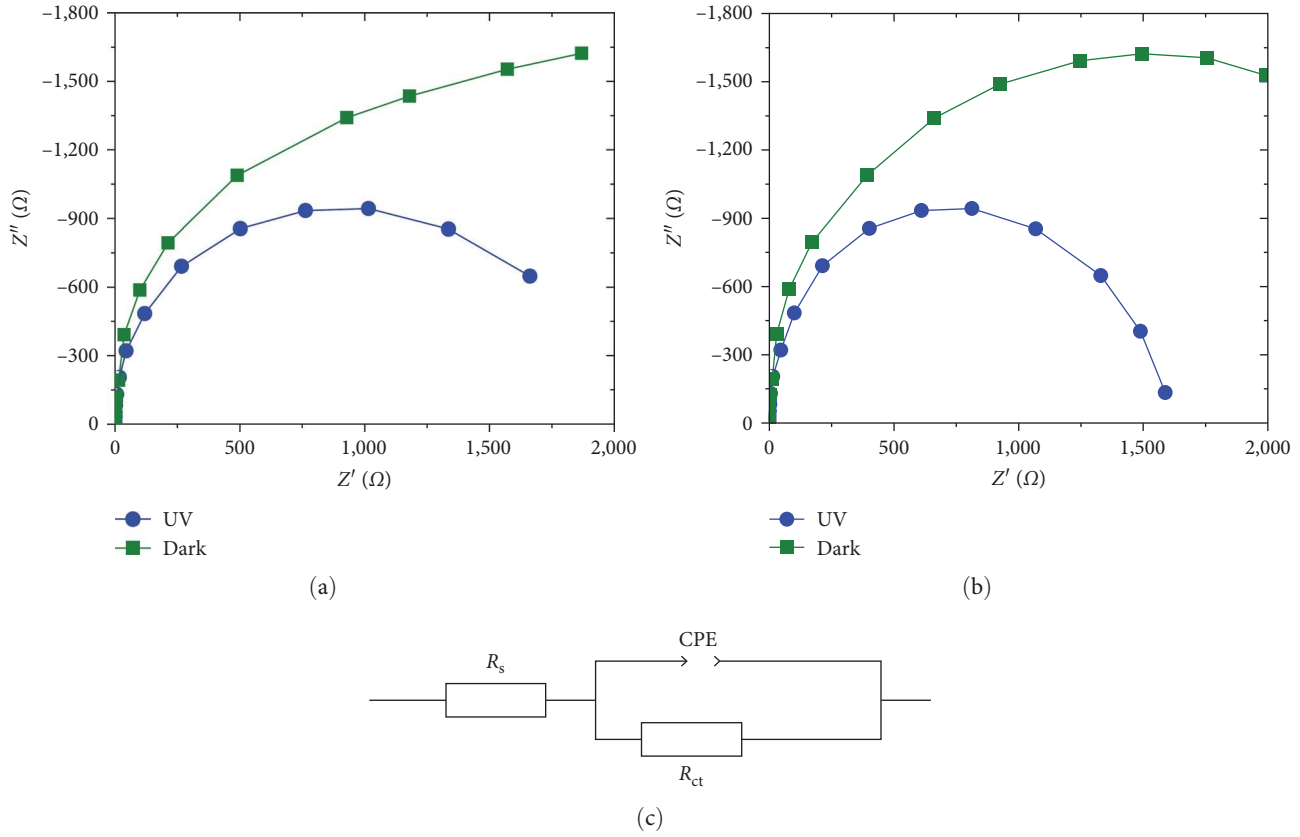

Figure 7: Nyquist plots for (a) photoanode A and (b) photoanode AB at an amplitude of 10 mV at the open circuit potential within a frequency range between 10 Hz and 100 KHz with a decreasing scanning frequency order in the dark, then under illumination UVA. (c) A simplified equivalent circuit model.

reference value for the energy gap of anatase-type titanium oxide, $E_g = 3.22$ eV and Degussa P25 $E_g = 3.15$ eV reported in the literature [36–38], indicating a quantum size effect into bandgap. This shift of the TiO_2 film bandgap caused by quantum confinement in thin layers has been thoroughly explained in a publication by King et al. [39]. The decrease in the energy gap with the decrease in the size of the particles is an interesting result. Many studies indicate that the decrease in the size is accompanied by an increase in the energy gap when P25 is added [5, 30]. Other studies indicate slight changes in the energy gap when the size of the particle decrease; this may be due to the effect of surfactant material, the combination ratio of anatase and rutile phases in the sample, and the viscosity of the solution in sol–gel method [29, 30].

3.3. Photo EC Properties. The present study involved a photoelectrochemical investigation of anodes through EIS measurements under both UVA illumination ($\lambda = 360$ nm) and dark conditions. This investigation was conducted in a three-electrode cell that featured a flat quartz window opposite the working electrode, which had an exposed front face electrode area of 2 cm^2. The experimental setup employed Ag/AgCl as the reference electrode and a Pt wire as the working electrode.

Figures 7(a) and 7(b) depict the Nyquist plots obtained using a 10 mV amplitude at the open circuit potential within a frequency range of 10 Hz–100 KHz, with a decreasing scanning frequency order, first in the dark and then under UVA illumination. Nyquist plots convey information on the charge transfer process as the diameters of the semicircles are equal to the charge transfer resistance of a sample [40]. As seen in Figure 7, all plots obtained under UVA illumination exhibit semicircles similar to those obtained in the dark. Notably, the semicircle diameter of the anodes under illumination is smaller than that of the same films in the dark. This observation suggests that the charge transfer rate under illumination is higher than that in the dark for the anodes. For anode AB, obtained by the addition of titanium nanooxide Degussa P25, the charge transfer rate under both dark and illumination conditions is higher than that of anode A, indicating an enhanced charge conductivity. The charge transfer resistance can be determined by fitting the arc radius of the Nyquist curves according to the proposed equivalent circuit illustrated in Figure 7(c). The components of the circuit, R_s, CPE, and R_{ct}, represent the series resistance, constant phase element, and charge transfer resistance, respectively.

Figure 8 illustrates that no significant dark current was detected, even at high potential, while substantial photocurrent densities were observed under illumination on both A

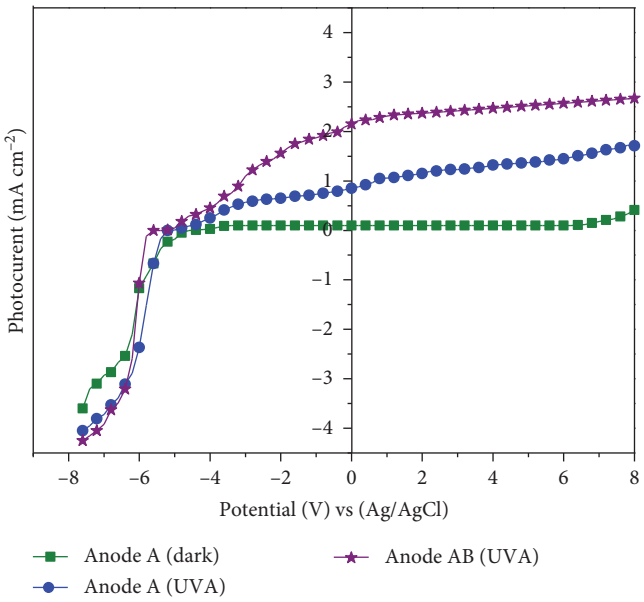

FIGURE 8: Linear-sweep voltammograms: (a) photoanode A in the dark; (b) photoanode A under illumination UVA; (c) photoanode AB under illumination UVA.

and AB photoelectrodes. It was observed that the photocurrent increased linearly with the applied potential bias until eventually reaching a plateau. Notably, the AB anode displayed significantly higher photocurrent density compared to the pristine A anode.

Based on the EIS and photocurrent measurements, it can be concluded that both anodes, with and without the addition of titanium nanooxide, exhibit significant photo-generated currents under UVA illumination, indicating their potential suitability as photoanodes. Furthermore, the AB anode displays a more active surface, which can be attributed to its higher surface roughness, uniform coverage of the substrate surface, and increased photocurrent density. These properties render it a promising candidate for use as a photoelectrocatalytic material electrode, which could play a crucial role in pollutant degradation.

3.4. Degradation of MB under UVA Light. Figure 9(a) illustrates the reduction of MB concentration over time using A and B anodes, while Figure 9(b)–9(f) presents the UV–Vis spectra of a 25 mg L^{-1} MB solution at various time intervals (0–240 min). The initial spectrum ($t = 0$), depicted in Figure 9(b), exhibits the characteristic peak of MB at 664 nm, which gives the aqueous MB solution its blue color [41].

The obtained results are in concurrence with previously reported findings [42]. As the reaction proceeded, the reaction solution gradually lost its color, and the absorption maximum at 664 nm decreased while shifting towards a shorter wavelength, approximately 600 nm after 240 min, due to the formation of demethylated dyes [43]. After 60 min of reaction with MB, the λ_{max} of AB photoanode shifted to 654 nm, resembling that of Azure B (AB). After 120 min, λ_{max} shifted to 630 nm, which is similar to the λ_{max} of Azure A (AA). After 180 min, λ_{max} shifted to 615 nm, which corresponds to the λ_{max} of Azure C (AC), and after 240 min, λ_{max} shifted to 600 nm, which is comparable to the λ_{max} of Thionin (Th). These observations align with those reported in a publication by Yogi et al. [44]. The photocatalytic reaction mechanism involves the reaction of MB with generated $HO^{\cdot}$ radicals or h^{+}, leading to the *N*-demethylation of its auxochromic dimethylamine groups. This demethylation results in the degradation of MB into a compound with a shorter absorption wavelength, along with H_2O and CO_2 [45]. Figure 10 shows the intermediates formed during the demethylation of MB in the PEC process using AB photoanode [44].

The treatment was performed at pH = 7, as indicated by our previous results, which showed that pH 7 provides the optimal MB dissociation value; since pHzpc TiO_2 < pH = 7 (as shown in Table 1), titanium oxide acquires a negative charge [46], which enhances the adsorption affinity for MB (a cationic dye). Our results are consistent with prior research indicating that the addition of P25 can enhance the photoanodes' efficiency in degrading MB by improving the electron–hole pairs' separation efficiency, photocatalytic activity, and PEC performance [28–30]. Furthermore, the AB photoanode's operational durability was tested and found to withstand three cycles without breaking down or peeling off.

3.5. Kinetics of PEC Degradation of MB. In general, the PEC degradation of organic pollutants using TiO_2 film electrodes has been seen to follow first-order or pseudo-first-order kinetics and can be described by the Langmuir–Hinshelwood kinetic model. The kinetics data of the degradation of MB were analyzed using a first-order kinetic model [47].

$$\mathrm{Ln}\left(\frac{C_t}{C_0}\right) = -kt, \tag{3}$$

where C_t is the MB concentration (mg L^{-1}) at time t, C_0 is the MB initial concentration (mg L^{-1}), k is kinetic constants (min^{-1}), and t is the reaction time (min).

Table 1 presents the energy gaps, film thickness, pH zero-point charge, and the first-order kinetic constants for A and AB photoanodes during three cycles.

When the ln C_0/C vs time curve obtained at initial MB concentrations is plotted in Figure 11 for both anodes. The kinetic constant for the PEC degradation of MB using an AB anode was higher than that measured using an A anode (the former was 134×10^{-4} min^{-1} and the latter was 110×10^{-4} min^{-1}) for the first cycle as shown in Table 1. These results show that the crystal structures of titanium oxide and E_g can significantly influence the kinetic constant of degradation on PEC.

3.6. Application of A and AB Photoanodes in Different Technologies. The photoanodes A and AB being used as working electrodes to study their efficiency in removing MB in some of advanced oxidation processes. A comparison was made between the PEC technology, the PC technology (without turning on the current), and the EC technology (no

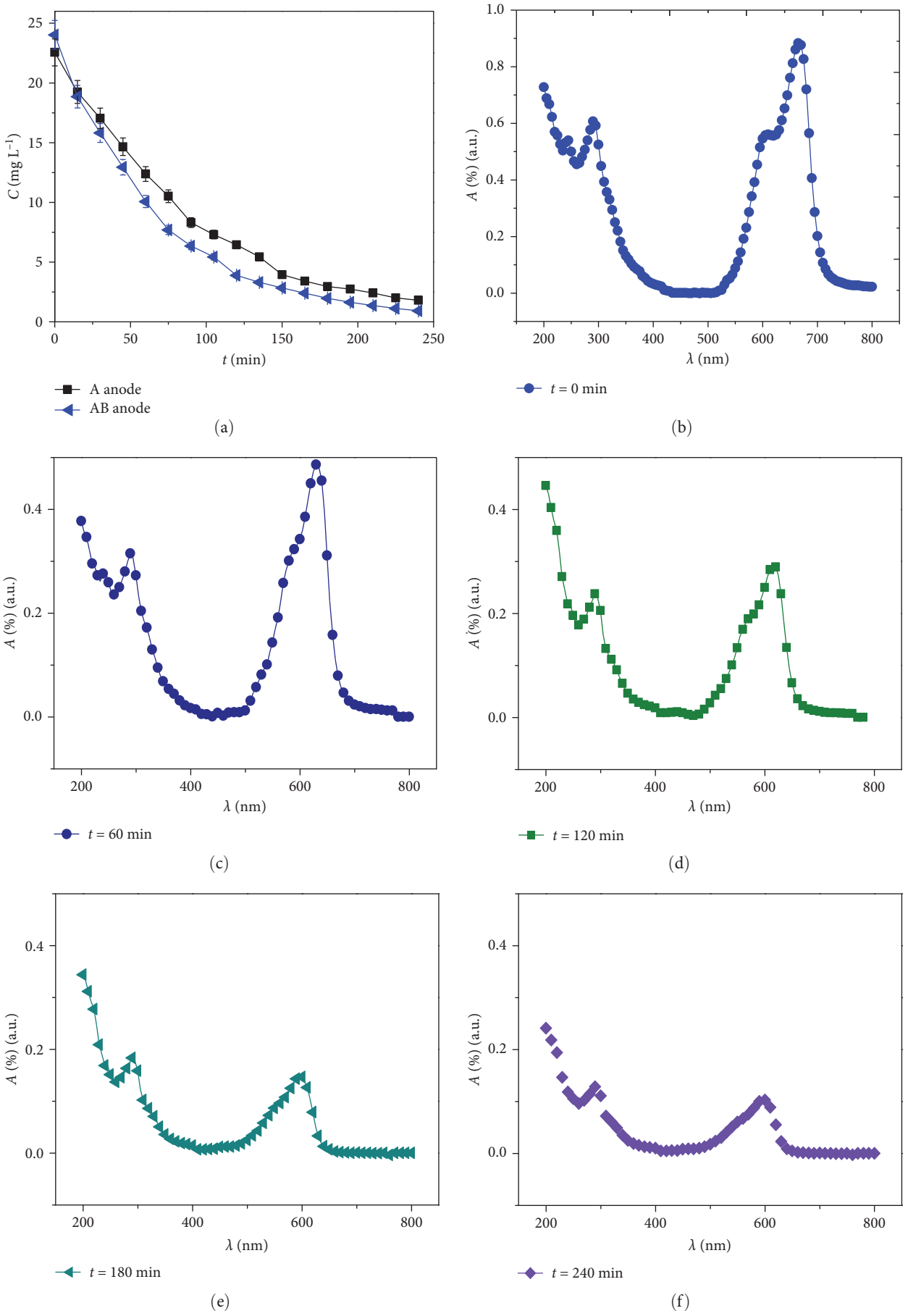

Figure 9: (a) Photoelectrocatalytic degradation of MB by A and AB photoanodes and (b)–(f) UV–Vis spectra of AB anode during treatment.

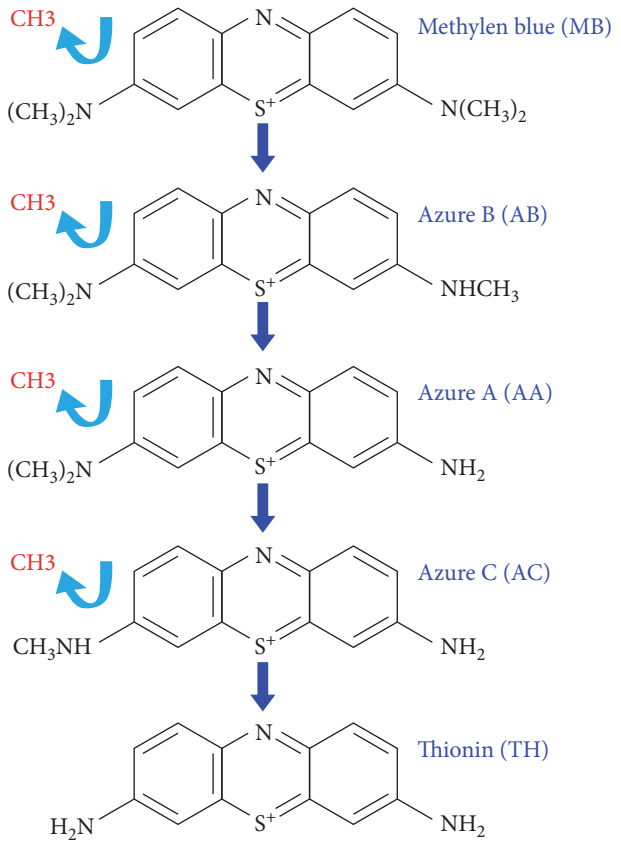

Figure 10: Demethylation reaction of MB [44].

Table 1: Results summary for A and AB photoanode for three cycles.

	A photoanode	AB photoanode
E_g	3.52 eV	3.35 eV
Thickness	230 nm	180 nm
pHzpc	6.1	6.32
K (min^{-1})		
First cycle (1)	$110 \times 10^{-4}(min^{-1})$	$134 \times 10^{-4}(min^{-1})$
Second cycle (2)	$104 \times 10^{-4}(min^{-1})$	$129 \times 10^{-4}(min^{-1})$
Third cycle (3)	$90 \times 10^{-4}(min^{-1})$	$125 \times 10^{-4}(min^{-1})$

light source), with the same treatment unit, to degradation of MB using the A and AB photoanodes and compared it with exposing the solution to UVA rays only photooxidation (PO). After 4 hr, percentages of the color removal and TOC were 2.1% and 0.4%, respectively, when exposing 200 mL of MB solution (25 mg L^{-1}) to ultraviolet light. And it is only caused by the PO of MB. The results in Table 2 showed that after 4 hr of treatment, the anode AB showed a greater percentage of removal of color and total organic carbon than the anode A in whole treatments, in addition to the superiority of the PEC for the three cycles over all the studied techniques. Despite the formation of strong oxidants agents as h^+, $^{\cdot}OH$ in PEC and PC, the superiority of PEC in removing MB color is due to the possibility of transferring the

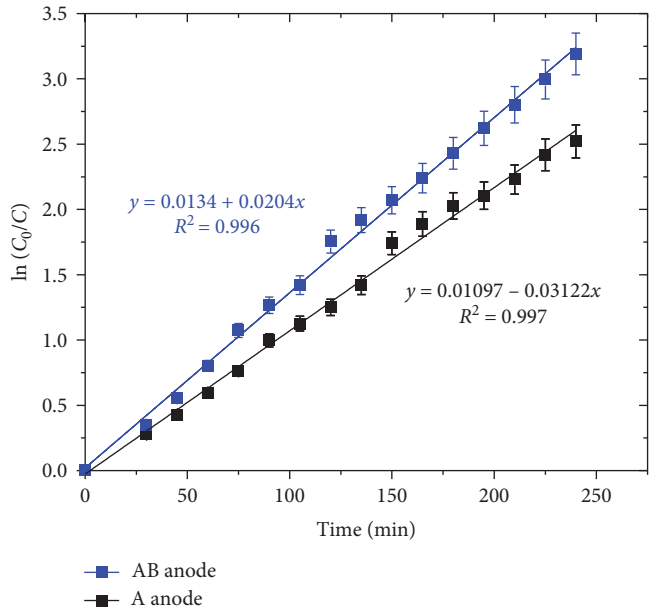

Figure 11: The first-order kinetics in the decolonization of MB on A and AB photoanodes for different reaction times for the first cycle.

Table 2: MB removal by using different treatment technologies.

Process	A photoanode		AB photoanode	
	Color removal (%)	TOC (%)	Color removal (%)	TOC (%)
PC	28	10.5	33	14
EC	19	10.2	21	12
PEC first cycle (1)	92	56	95.9	63
PEC second cycle (2)	89.1	52	94.8	61
PEC third cycle (3)	86.7	47	93.6	57.8

formed electron through the external circuit to the cathode, which inhibits the recombination of an electron–hole [47], and increases the amount of oxidants formed and thus greater removal of MB color.

4. Conclusion

In this study, TiO_2 was prepared on ITO glass via the sol–gel method to produce photoanodes labeled as AB and A, with and without the addition of titanium dioxide nanopowder (Degussa, P25) 70% anatase and 30% rutile phases, respectively. The surface morphology, photo EC, and optical properties of the prepared anodes were characterized using AFM, EIS, and UV–Vis spectroscopy. The optical studies revealed that the bandgap energy (E_g) ranged from 3.50 to 3.35 eV, and the size of the titanium dioxide particles decreased from 125 to 75 nm. The PEC performance of anodes A and AB was investigated via the degradation of MB under UV light irradiation, with photoanode AB demonstrating excellent performance. The efficiency of color removal and TOC were

95.9% and 63%, respectively, while it was 92% and 56% for photoanode A (without the addition of Degussa P25). The degradation of MB followed first-order kinetics for all anodes. In conclusion, anode AB achieved a higher removal rate than anode A when used in PC, EC, and PEC technologies, with PEC demonstrating the greatest degradation of MB. The present study proposes that TiO_2/ITO films could be a promising candidate as photoanodes with photocatalytic activity for the photoelectrocatalytic degradation of pollutants in wastewater under UV light irradiation, as the photoanode showed excellent results, and the materials are commercially available.

Data Availability

The datasets used and/or analyzed during the current study are available from the corresponding author upon request.

Conflicts of Interest

The authors declare that they have no conflicts of interest.

References

[1] E. Brillas and C. A. Martínez-Huitle, "Decontamination of wastewaters containing synthetic organic dyes by electrochemical methods. An updated review," *Applied Catalysis B: Environmental*, vol. 166-167, pp. 603–643, 2015.

[2] B. O. Orimolade and O. A. Arotiba, "Enhanced photoelectrocatalytic degradation of diclofenac sodium using a system of Ag–$BiVO_4$/BiOI anode and Ag–BiOI cathode," *Scientific Reports*, vol. 12, Article ID 4214, 2022.

[3] B. O. Orimolade and O. A. Arotiba, "Towards visible light driven photoelectrocatalysis for water treatment: application of a FTO/$BiVO_4$/Ag_2S heterojunction anode for the removal of emerging pharmaceutical pollutants," *Scientific Reports*, vol. 10, Article ID 5348, 2020.

[4] P. Alulema-Pullupaxi, P. J. Espinoza-Montero, C. Sigcha-Pallo et al., "Fundamentals and applications of photoelectrocatalysis as an efficient process to remove pollutants from water: a review," *Chemosphere*, vol. 281, Article ID 130821, 2021.

[5] S. Garcia-Segura and E. Brillas, "Applied photoelectrocatalysis on the degradation of organic pollutants in wastewaters," *Journal of Photochemistry and Photobiology C: Photochemistry Reviews*, vol. 31, pp. 1–35, 2017.

[6] Q. Q. Cai, B. C. Y. Lee, S. L. Ong, and J. Y. Hu, "Fluidized-bed Fenton technologies for recalcitrant industrial wastewater treatment—recent advances, challenges and perspective," *Water Research*, vol. 190, Article ID 116692, 2021.

[7] P. R. Yaashikaa, M. Keerthana Devi, and P. Senthil Kumar, "Engineering microbes for enhancing the degradation of environmental pollutants: a detailed review on synthetic biology," *Environmental Research*, vol. 214, Part 1, Article ID 113868, 2022.

[8] H. Yan, C. Lai, D. Wang et al., "*In situ* chemical oxidation: peroxide or persulfate coupled with membrane technology for wastewater treatment," *Journal of Materials Chemistry A*, vol. 9, no. 20, pp. 11944–11960, 2021.

[9] P. Alulema-Pullupaxi, L. Fernández, A. Debut et al., "Photoelectrocatalytic degradation of glyphosate on titanium dioxide synthesized by sol–gel/spin-coating on boron doped diamond (TiO_2/BDD) as a photoanode," *Chemosphere*, vol. 278, Article ID 130488, 2021.

[10] C. Sigcha-Pallo, J. M. Peralta-Hernández, P. Alulema-Pullupaxi et al., "Photoelectrocatalytic degradation of diclofenac with a boron-doped diamond electrode modified with titanium dioxide as a photoanode," *Environmental Research*, vol. 212, Part C, Article ID 113362, 2022.

[11] G. G. Bessegato, J. C. Cardoso, and M. V. B. Zanoni, "Enhanced photoelectrocatalytic degradation of an acid dye with boron-doped TiO_2 nanotube anodes," *Catalysis Today*, vol. 240, Part A, pp. 100–106, 2015.

[12] E. Zarei and R. Ojani, "Fundamentals and some applications of photoelectrocatalysis and effective factors on its efficiency: a review," *Journal of Solid State Electrochemistry*, vol. 21, pp. 305–336, 2017.

[13] I. Tantis, M. V. Dozzi, L. G. Bettini et al., "Highly functional titania nanoparticles produced by flame spray pyrolysis. Photoelectrochemical and solar cell applications," *Applied Catalysis B: Environmental*, vol. 182, pp. 369–374, 2016.

[14] M. Zhang, T. Chen, and Y. Wang, "Insights into TiO_2 polymorphs: highly selective synthesis, phase transition, and their polymorph-dependent properties," *RSC Advances*, vol. 7, no. 83, pp. 52755–52761, 2017.

[15] A. H. Jawad, N. S. A. Mubarak, M. A. M. Ishak, K. Ismail, and W. I. Nawawi, "Kinetics of photocatalytic decolourization of cationic dye using porous TiO_2 film," *Journal of Taibah University for Science*, vol. 10, no. 3, pp. 352–362, 2016.

[16] A. Kruth, S. Peglow, A. Quade et al., "Structural and photoelectrochemical properties of DC magnetron-sputtered TiO_2 layers on FTO," *The Journal of Physical Chemistry C*, vol. 118, no. 43, pp. 25234–25244, 2014.

[17] Q. Zhang and C. Li, "TiO_2 coated ZnO nanorods by mist chemical vapor deposition for application as photoanodes for dye-sensitized solar cells," *Nanomaterials*, vol. 9, no. 9, Article ID 1339, 2019.

[18] Y. Zhao, L. Zhang, J. Liu et al., "Atomic/molecular layer deposition for energy storage and conversion," *Chemical Society Reviews*, vol. 50, no. 6, pp. 3889–3956, 2021.

[19] S. Dosta, M. Robotti, S. Garcia-Segura, E. Brillas, I. G. Cano, and J. M. Guilemany, "Influence of atmospheric plasma spraying on the solar photoelectro-catalytic properties of TiO_2 coatings," *Applied Catalysis B: Environmental*, vol. 189, pp. 151–159, 2016.

[20] R. Sharma, A. Sarkar, R. Jha, A. K. Sharma, and D. Sharma, "Sol–gel–mediated synthesis of TiO_2 nanocrystals: structural, optical, and electrochemical properties," *International Journal of Applied Ceramic Technology*, vol. 17, no. 3, pp. 1400–1409, 2020.

[21] H. Zhang and C. Cheng, "Three-dimensional FTO/TiO_2/$BiVO_4$ composite inverse opals photoanode with excellent photoelectrochemical performance," *ACS Energy Letters*, vol. 2, no. 4, pp. 813–821, 2017.

[22] G.-C. Fan, Y. Lu, H. Zhao, Q. Liu, Z. Li, and X. Luo, "Photoelectrochemical cell enhanced by ternary heterostructured photoanode: toward high-performance self-powered cathodic cytosensing," *Biosensors and Bioelectronics*, vol. 137, pp. 52–57, 2019.

[23] R. Tang, S. Zhou, Z. Zhang, R. Zheng, and J. Huang, "Engineering nanostructure–interface of photoanode materials toward photoelectrochemical water oxidation," *Advanced Materials*, vol. 33, no. 17, Article ID 2005389, 2021.

[24] R. Dom, S. Govindarajan, S. V. Joshi, and P. H. Borse, "A solar-responsive zinc oxide photoanode for solar-photon-harvester

photoelectrochemical (PEC) cells," *Nanoscale Advances*, vol. 2, no. 8, pp. 3350–3357, 2020.

[25] M. A. Majeed Khan, R. Siwach, S. Kumar, and A. N. Alhaza, "Role of Fe doping in tuning photocatalytic and photoelectrochemical properties of TiO_2 for photodegradation of methylene blue," *Optics & Laser Technology*, vol. 118, pp. 170–178, 2019.

[26] M.-Z. Ge, C.-Y. Cao, S.-H. Li et al., "*In situ* plasmonic Ag nanoparticle anchored TiO_2 nanotube arrays as visible-light-driven photocatalysts for enhanced water splitting," *Nanoscale*, vol. 8, no. 9, pp. 5226–5234, 2016.

[27] I. Olvera-Rodríguez, R. Hernández, A. Medel et al., "TiO_2/Au/TiO_2 multilayer thin-film photoanodes synthesized by pulsed laser deposition for photoelectrochemical degradation of organic pollutants," *Separation and Purification Technology*, vol. 224, pp. 189–198, 2019.

[28] L. Andronic, D. Perniu, and A. Duta, "Synergistic effect between TiO_2 sol–gel and Degussa P25 in dye photodegradation," *Journal of Sol–Gel Science and Technology*, vol. 66, pp. 472–480, 2013.

[29] X. Guo, L. Rao, P. Wang et al., "Photocatalytic properties of P25-doped TiO_2 composite film synthesized *via* sol–gel method on cement substrate," *Journal of Environmental Sciences*, vol. 66, pp. 71–80, 2018.

[30] F. Oshani, R. Marandi, S. Rasouli, and M. K. Farhoud, "Photocatalytic investigations of TiO_2–P25 nanocomposite thin films prepared by peroxotitanic acid modified sol–gel method," *Applied Surface Science*, vol. 311, pp. 308–313, 2014.

[31] M. I. Carreño-Lizcano, A. F. Gualdrón-Reyes, V. Rodríguez-González, J. A. Pedraza-Avella, and M. E. Niño-Gómez, "Photoelectrocatalytic phenol oxidation employing nitrogen doped TiO_2–rGO films as photoanodes," *Catalysis Today*, vol. 341, pp. 96–103, 2020.

[32] B. M. Babić, S. K. Milonjić, M. J. Polovina, and B. V. Kaludierović, "Point of zero charge and intrinsic equilibrium constants of activated carbon cloth," *Carbon*, vol. 37, no. 3, pp. 477–481, 1999.

[33] J. B. Coulter and D. P. Birnie III, "Assessing Tauc plot slope quantification: ZnO thin films as a model system," *Physica Status Solidi (b)*, vol. 255, no. 3, Article ID 1700393, 2018.

[34] A. V. Vorontsov and H. Valdés, "Quantum size effect and visible light activity of anatase nanosheet quantum dots," *Journal of Photochemistry and Photobiology A: Chemistry*, vol. 379, pp. 39–46, 2019.

[35] M. I. Khan, K. A. Bhatti, R. Qindeel, Fazal-e-Aleem, Naeem-ur-Rehman, and N. Alonizan, "Sol–gel deposition and characterization of multilayer 2% Cu doped TiO_2 nano structured thin films," *Journal of Materials Science: Materials in Electronics*, vol. 28, pp. 9471–9477, 2017.

[36] M. Mehrabi and V. Javanbakht, "Photocatalytic degradation of cationic and anionic dyes by a novel nanophotocatalyst of TiO_2/$ZnTiO_3$/αFe_2O_3 by ultraviolet light irradiation," *Journal of Materials Science: Materials in Electronics*, vol. 29, pp. 9908–9919, 2018.

[37] D. Jiang, T. A. Otitoju, Y. Ouyang et al., "A review on metal ions modified TiO_2 for photocatalytic degradation of organic pollutants," *Catalysts*, vol. 11, no. 9, Article ID 1039, 2021.

[38] R. Trejo-Tzab, J. J. Alvarado-Gil, and P. Quintana, "Photocatalytic activity of Degussa P25 TiO_2/Au obtained using argon (Ar) and nitrogen (N_2) plasma," *Topics in Catalysis*, vol. 54, pp. 250–256, 2011.

[39] D. M. King, X. Du, A. S. Cavanagh, and A. W. Weimer, "Quantum confinement in amorphous TiO_2 films studied via atomic layer deposition," *Nanotechnology*, vol. 19, no. 44, Article ID 445401, 2008.

[40] A. R. Bredar, A. L. Chown, A. R. Burton, and B. H. Farnum, "Electrochemical impedance spectroscopy of metal oxide electrodes for energy applications," *ACS Applied Energy Materials*, vol. 3, no. 1, pp. 66–98, 2020.

[41] G. Xia, Y. Lu, X. Gao, C. Gao, and H. Xu, "Electro-Fenton degradation of methylene blue using polyacrylonitrile-based carbon fiber brush cathode," *CLEAN—Soil, Air, Water*, vol. 43, no. 2, pp. 229–236, 2015.

[42] U. Mahanta, M. Khandelwal, and A. S. Deshpande, "TiO_2@SiO_2 nanoparticles for methylene blue removal and photocatalytic degradation under natural sunlight and low-power UV light," *Applied Surface Science*, vol. 576, Part A, Article ID 151745, 2022.

[43] P. Zhang, Y. Zhan, B. Cai et al., "Shape-controlled synthesis of Mn_3O_4 nanocrystals and their catalysis of the degradation of methylene blue," *Nano Research*, vol. 3, pp. 235–243, 2010.

[44] C. Yogi, K. Kojima, N. Wada et al., "Photocatalytic degradation of methylene blue by TiO_2 film and Au particles-TiO_2 composite film," *Thin Solid Films*, vol. 516, no. 17, pp. 5881–5884, 2008.

[45] T. Zhang, T. Oyama, A. Aoshima, H. Hidaka, J. Zhao, and N. Serpone, "Photooxidative *N*-demethylation of methylene blue in aqueous TiO_2 dispersions under UV irradiation," *Journal of Photochemistry and Photobiology A: Chemistry*, vol. 140, no. 2, pp. 163–172, 2001.

[46] D. Liu, R. Tian, J. Wang et al., "Photoelectrocatalytic degradation of methylene blue using F doped TiO_2 photoelectrode under visible light irradiation," *Chemosphere*, vol. 185, pp. 574–581, 2017.

[47] M. Natsir, Y. I. Putri, D. Wibowo et al., "Effects of Ni–TiO_2 pillared clay–montmorillonite composites for photocatalytic enhancement against reactive orange under visible light," *Journal of Inorganic and Organometallic Polymers and Materials*, vol. 31, pp. 3378–3388, 2021.